Optimizing Turbine Siting and Wind Farm Layout in Indonesia

I. Ifanda*‡, Didik Rostyono*, Rudi Purwo Wijayanto*, Nurry Widya Hesty*, Amiral Aziz*‡, Khotimatul Fauziah*, Toha Zaky*, Ario Witjakso*, Ahmad Fudholi*,**‡

*Research Center for Conversion and Conservation Energy, National Research and Innovation Agency Republic of Indonesia (BRIN), South Tangerang 15314 Indonesia

**Solar Energy Research Institute, Universiti Kebangsaan Malaysia, 43600 Bangi, Selangor, Malaysia

(ifanda@brin.go.id, didi007@brin.go.id, rudi014@brin.go.id, nurr010@brin.go.id, amiral.aziz@brin.go.id, khot001@brin.go.id, toha002@brin.go.id, ario001@brin.go.id, ahmad.fudholi@brin.go.id)

‡Corresponding Author; Ifanda, Amiral Aziz, Ahmad Fudholi, Research Center for Conversion and Conservation Energy, National Research and Innovation Agency Republic of Indonesia (BRIN), South Tangerang 15314,

ifanda@brin.go.id, amiral.aziz@brin.go.id, a.fudholi@ukm.edu.my

Received: 01.04.2023 Accepted:20.05.2023

Abstract- Wind resource assessments are required to identify a specific area capable of producing valuable energy from wind speeds. This paper aims to optimize wind assessment through wind farm siting and layout in Indonesia's semi-arid region. Wind data collected on Sumba Island over a one-year period was analyzed to assess the area's wind energy potential. Wind Atlas Analysis and Application Programme (WAsP) and Windographer were used to generate a generalized wind climate and resource maps for the area. Wind farm layout and preliminary turbine micro-sitting were completed with various scenarios in mind to achieve the best possible result. Four different scenarios are considered to maximize power output. There are 34 identical wind turbines with a unit capacity of 90 kW in Scenario 1. Scenario 2 includes 20 identical wind turbines with a total capacity of 3000 kW. In Scenario 3, 14 identical wind turbines with 225 kW of unit capacity are used. There are 12 identical wind turbines with a unit capacity of 250 kW in Scenario 4. The results showed that Scenario 1 produced the highest total net Annual Energy Production (AEP) of 11,287 MWh/year with a 3.73% wake loss. The minimum wake loss seemed to be 2.62% in Scenario 4, with a total net AEP of 10,221 MWh/year.

Keywords Wind resource assessment, semi-arid region, WAsP, wake loss.

1. Introduction

One of the main factors influencing every country's progress is its access to energy. A country's ability to maintain its energy utilization is a key factor in its success [1]. According to Tang et al. [2], the utilization of renewable energy has grown globally over time because of the need to adhere to international climate agreements that forbid the use of fossil fuels as an energy source. Wind energy has recently emerged as the leading sustainable energy alternative for reducing the effects of energy on anthropogenic pollutants in the atmosphere, with a total installed capacity of 651 GW worldwide in 2019 [3]. As a rapidly developing economy, Indonesia has set a target of 23% renewable energy in its total energy mix by 2025, as stated in the National Electricity Master Plan (RUKN), as well as a reduction in greenhouse gas emissions of 29–41% by 2030 and net-zero emissions by 2060. To meet the target, several studies assessing renewable energy potential have been conducted. Hesty et al. [4] estimate the national wind energy potential, while Pranoto et al. [5] estimate the hydro energy potential. A web-based application has been created to calculate the energy potential of a rooftop solar PV system installed on a home by Nurliyanti et al. [6]. According to the Indonesian Ministry of Mineral and Energy Resources (MMER), the total solar energy potential in Indonesia is 3,294.36 gigatons peak (GWp), which is distributed evenly across the country. East Nusa Tenggara (369.5 GWp), Riau (290.41 GWp), and South Sumatra (285.1

GWp) are the three provinces with the greatest solar energy potential. MMER estimates that Indonesia has 154.88 GW of wind energy potential, with onshore potential of 60.65 GW and offshore potential of 94.2 GW. Onshore locations with high wind energy potential, including wind speeds of 6–8 m/s, power densities of 400–500 W/m^2, and AEP of 4-5 GWh/year, can be found on the south coast of Java, South Sulawesi, Maluku, and East Nusa Tenggara.

East Nusa Tenggara province, particularly Sumba Island, has more than 200 MW of wind energy potential, with wind speeds ranging from 5 to 9 m/s. Sumba also had solar energy potential due to its daily solar insolation of 5 kWh/m^2 [7]. Sumba was designated as the Iconic Island of Renewable Energy (RE) by a ministerial decree in 2015. The island's sparsely populated settlements and huge open savannah plains provide plenty of open space for the construction of wind and solar farms. Sumba, like the rest of Indonesia, has only two seasons: dry and rainy. Indonesia's climate and wind surface direction are mostly influenced by the Asian-Australian Monsoon (AAM) system [8]. According to Alifdini [9], the Asian (Australian) monsoon is distinguished by a northwesterly (southerly) wind that blows from Asia (Australia) to Australia (Asia), bringing humid (dry) air and creating a rainy (dry) season in the majority of Indonesian regions. Due to its wind patterns, the AAM system is also known as the northeast monsoon (rainy season), which peaks from December to February, and the southwest monsoon (dry season), which peaks from June to August. Because of its lengthy dry season, which lasts from April through November (7 months) every year, Sumba is considered a dry island with an unusually semi-arid climate [10]. Sumba, as a semi-arid region, receives the least rainfall in the country. The monsoon brings steady, strong winds from June to August, while from December to April it brings calm winds.

Despite Sumba's high renewable energy potential, the region's energy security index remains low [11]. Sumba's electrical system currently consists of three electrical systems: East Sumba, West Sumba, and Southwest Sumba. All these systems rely heavily on diesel power plants spread across Sumba Island. According to PLN's (Indonesia's state utility) long-awaited 2021–2030 Electricity Supply Business Plan (RUPTL), a total capacity of approximately 42 MW of various thermal and renewable power plants is planned for the island of Sumba, with a total wind power generation capacity of 3 MW. RUPTL also indicates that a 70 kV transmission line and 70 kV substations will be built to improve power transmission efficiency between the east and west Sumba systems. The potential for wind power generation at any scale, whether for grid-connected or stand-alone systems, must be thoroughly assessed [12,13]. Furthermore, the optimal use of the available wind resources and the viability of a wind power project depend on the siting of the wind turbines as described by Mathew [14] and Manwell et al. [15]. A precise and accurate analysis of the data for the relevant area is required to construct the wind farm to its full potential [16]. Numerous in-depth scientific studies on wind energy have recently been undertaken on a global scale. In order to enhance wind speed forecasting techniques for the wind pattern over complex terrain, Flay et al. [17] employed CFD, Wind Atlas Analysis and Application Program (WAsP) models, and wind-tunnel testing in New Zealand's established infrastructure. WAsP was used to assess the wind power potential in Turkey's Mardin province, as well as the potential to meet specific energy demands [18]. Kamdar et al. [19] investigated wind energy potential using WAsP Tool for a small–scale wind farm in south–eastern Thailand. Ratjiranukool [20] used the Weather Research and Forecasting (WRF) meso-scale climate model to assess the wind energy potential of Thailand's northern region. Meanwhile, Wang et al. [21] proposed wind energy potential assessment method based on wind speed, wind direction and its power using finite mixture statistical distributions. Kwon [22] presented uncertainty analysis of wind energy potential assessment using probability models and Monte-Carlo based simulation procedure. Moreover, several studies on predicting wind energy production using machine learning methods have also been developed to improve forecasting accuracy [23,24].

Studies on the investigation of wind energy based on the use of simulation software have gained attention in recent years. The programs utilized for wind energy can be used to assess the preliminary economic and technical viability of the projected investments. One of the most significant design challenges is the high initial investment cost of wind farms, which could result in significant financial losses if the feasibility analysis is flawed. WAsP is a well-known wind energy application program and a powerful tool for assessing wind resources. However, there has been little research on the application of the WAsP model to wind resource assessment in semi-arid areas. Using a methodology that complies with international standards, this research will offer a scientific method for evaluating wind resources in semi-arid regions like Sumba Island. According to the authors' knowledge, there is a gap in the literature regarding optimizing wind assessment through wind farm siting and layout using the WAsP tool in the semi-arid region. The WAsP and Windographer tools were used in this study to optimize wind farm siting and layout after a thorough analysis of the wind resources. The WAsP simulation calculates the mean wind speed and power density for selected eastern Sumba locations. The power and capacity factors of the sites with different wind turbine capacities were calculated and analyzed. This will enable decision-makers to set goals about how to meet rising power demands through renewable wind power. Furthermore, this study will contribute to the National Electricity Master Plan, which aims to replace fossil fuels with up to 23% renewable energy in its total energy mix by 2025. The paper discusses some results of the study that was conducted to optimize the turbine siting and wind farm layout in the semi-arid region of Indonesia.

2. Material and Methods

2.1. Description of Object Study

This research was carried out in Hambapraing, East Sumba Regency. Sumba Island has a semi-arid climate type with a short rainy season that lasts only for four months (December to March) and total annual rainfall of 547 mm up to 1100 mm during the period of 2018-2022 (statistics of Sumba Timur Regency 2018, 2019, 2020, 2021, 2022). According to statistics for Sumba Timur Regency (2022), the

average temperature varies between 36 C in October and 18 C in July. The average rainfall in East Sumba Regency in 2021 was 102.17 mm, with the highest level in March at 286 mm. Despite the fact that the most rain fell in March, the most rainy days occurred in January, with 25 days in contrast; from April to November, there was very little rain in East Sumba Regency. The short, wet season with little rainfall results in limited water availability. This area is characterized by a vast expanse of savanna and short thorny plants that reflect the nature of the region's dry climate, which deteriorates continuously due to successive drought years. with soils containing sand, limestone, and coral rock. The brittle rock, limestone, and soil in the area, which are unable to withstand the force of the winds that carry the bits of disintegrating material, are another problem. Due to stiff winds during the dry months, there is a phenomenon where sand accumulates in some areas.

The measuring mast is at 9° 31' 5.82" S latitude and 120° 10' 3.01" E longitude, with a height of 100 meters above sea level as shown in Fig. 1. Meteorological instruments such as anemometers, wind vane, barometric pressure, thermometers, rain gauges, and hygrometers are housed in the measuring mast. From September 2014 to September 2015, the instrument measured and recorded a 10-min average of wind speed and direction, solar radiation, temperature, and air pressure, as given in Table 1, which are primarily considered over an international standard period for wind measurement [25].

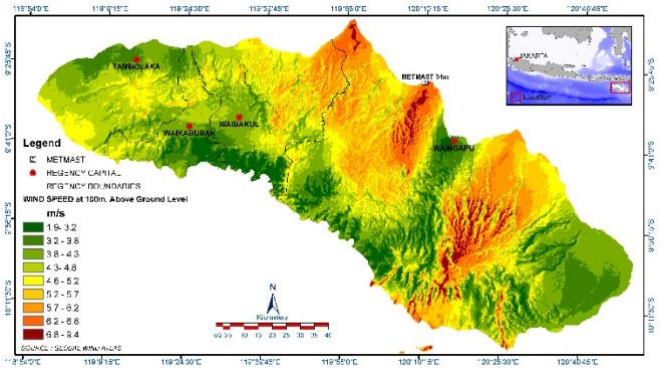

Fig. 1. The wind speed map for Sumba Island.

Table 1. Data set description of the location

Parameter	Unit	Value
Average wind speed (m/s)	m/s	6.16
Max wind speed (m/s)	m/s	19.3
Min wind speed (m/s)	m/s	0.4
Average Wind direction	°	128
Average temperature	°C	26.8
Average Solar Radiation	W/m^2	250
Average Barometric Pressure	mB	998

2.2. Methodology

The optimum wind farm layout should maximize energy production from an energy standpoint. This is mostly accomplished in wind farms by efficiently spreading the distance between wind turbines within the available region, maximizing the available wind resource while minimizing wake loss. However, from an economic standpoint, an optimized wind farm layout is one that minimizes the unit cost of produced energy. This is mostly accomplished by examining the trade-off between the energy yield benefits from increased wind turbine spacing and the greater expenditures associated with the land costs, the electrical cabling costs, and losses. Because the central part of Sumba where the wind farm is proposed is barren and uninhabited, land prices are not an important consideration in the optimization process. In this study, we solely apply single-objective optimization to reduce the total wake effect of the wind turbine farm, without taking into account the cost of connecting between wind turbines.

Figure 2 shows the flow diagram of this study. The main goal is to optimize the geographical location of every single WT (wind turbine) in the selected region, including its capacity, capacity factor, and AEP. The objective function is to minimize the wake effect of the WT's array on the wind farm. Referring to Azlan [26], some previous studies have provided several guidelines prior to WT positionings, such as land availability, forbidden zones, maximum investment, WT quantity and capacity, WT spacing, and electrical infrastructure. In this study, we consider capacity and spacing. There is no issue regarding land availability or forbidden zones on Sumba Island since it is a semi-arid region with no conservation area. This research was carried out in Hambapraing, East Sumba Regency. Sumba Island has a semi-arid climate type with a short rainy season that lasts only for four months (December to March), with a total annual rainfall of 547 mm up to 1100 mm during the period of 2018–2022.

We performed two types of preprocessing to simplify the optimization algorithm. Firstly, the geospatial location and its information regarding the wind potential; and secondly, we did image manipulation by dividing it into the number of rows and columns. The geospatial location and information refer to the Indonesia Geospatial Information Agency (BIG) via DEMNAS with the numbers 2106-13 and 2106-41, and a map of Sumba Timur is used as the data map reference. The number of rows and columns in the matrix of a wind farm represents the location of a single wind turbine. The distance between the columns is the spacing between two neighboring wind turbines or crosswind spacing. Meanwhile, the distance between two rows indicates the spacing between the turbines in the downstream direction or downwind spacing. Its spacing depends on the WT diameter, which means that influenced by capacity, a higher WT capacity usually has a wider diameter. The crosswind spacing is between 4D and 6D, and the downwind spacing is almost twice that, between 8D and 12D. The priority and non-priority of a single location of WT are decided by its potential energy based on the annual wind velocity.

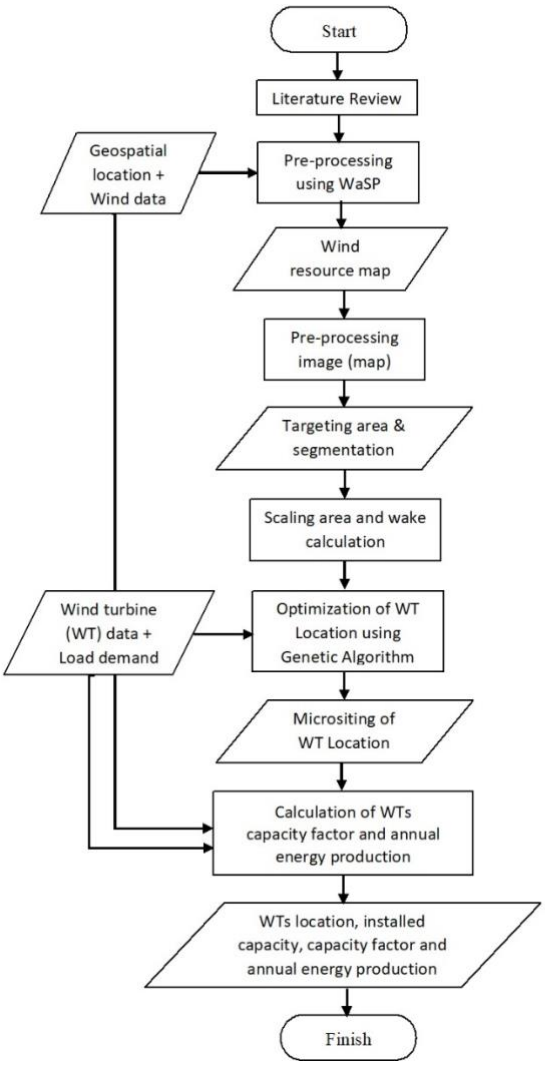

Fig. 2. Flow diagram of the study.

Figure 3 shows the two preprocessing datasets before feeding them to the optimization algorithm as a matrix. This research was carried out in Hambapraing, East Sumba Regency. Sumba Island has a semi-arid climate type with a short rainy season that lasts only for four months (December to March) and total annual rainfall of 547 mm up to 1100 mm during the period of 2018-2022 (statistics of Sumba Timur Regency 2018, 2019, 2020, 2021, 2022). According to statistics for Sumba Timur Regency (2022), the average temperature varies between 36 C in October and 18 C in July. The average rainfall in East Sumba Regency in 2021 was 102.17 mm, with the highest level in March at 286 mm.

We proposed a total capacity of 3 MW of WTs based on Indonesian electricity planning [RUPTL] for the region. Due to the limited facilities and infrastructure in the study region, including transportation, facilities, port capacity, bridges, roads, etc., it is not possible to choose a wind turbine with a unit capacity above 300 kW. A single WT capacity in this study is 90 kW, 150 kW, 225 kW, and 250 kW, which means we have four scenarios of a WT farm layout, and the total capacity for each scenario is about 3 MW. A 90 kW WT has a rotor diameter of 20 m, whereas a 250 kW WT's rotor diameter is 50 m. We set the crosswind spacing between 2D and 3D and the downwind spacing between 4D and 6D.

2.3. The Weibull Distribution

To design and select wind farms, wind speed is the main element that must be measured, while the performance of wind turbines is significantly influenced by the Weibull function probability distribution (PDF) [27]. In explaining the wind speed histogram, two parameters are often used in the calculation, namely the Weibull probability distribution. It is also used in the WAsP to study wind characteristics in all directions characterized by sectors [28]. The probability distribution function (PDF) of the Weibull distribution is defined by Eq. (1) [14,25,29]:

$$f(U) = \frac{k}{A} \times \left(\frac{U}{A}\right)^{k-1} \times e^{-\left(\frac{U}{A}\right)^{k}} \quad (1)$$

where $k > 0; U > 0; A > 0$.

The Weibull probability density function of observed wind speed U (m/s) is represented by $f(U)$, the Weibull scale parameter in m/s is defined by A, and the dimensionless Weibull shape parameter is represented by k. The Weibull shape parameter k has values between 1 and 3 and describes the behaviour of wind in accordance with its speed; where small values of k show variations in wind variables, a rather constant wind speed can be shown with a large k value [25,28].

Then, the Weibull distribution is expressed according to the cumulative probability function in Eq. (2) [30,31]

$$f(U) = 1 - e^{-\left(\frac{U}{A}\right)^{k}} \quad (2)$$

where $f(U)$ is the cumulative distribution function of the observed wind speed U. The cumulative distribution is the integral of the density or PDF with respect to speed [25].

2.4. Calculation of Wake Effect

The Jensen wake model is mostly used in previous studies, and other wake models are Gaussian or Frandsen [26]. The Jansen wake model is shown in Fig. 4 [32], there are no external forces acting upon the control volume and only the angular momentum is conserved inside the wake.

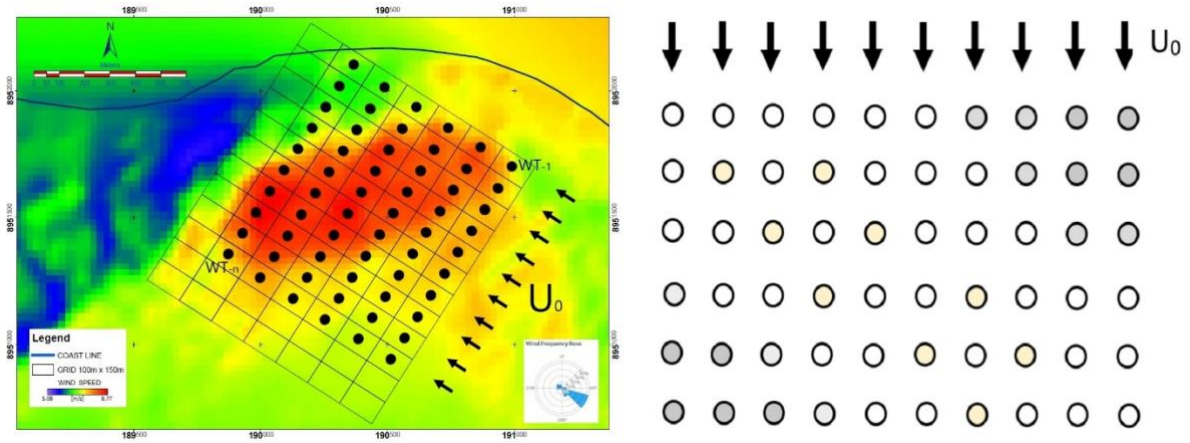

(a) (b)

Fig. 3. (a) Pre-processing using WAsP and (b) Pre-processing image with the value of the rectangular area to identify nonpriority and priority area as constraints.

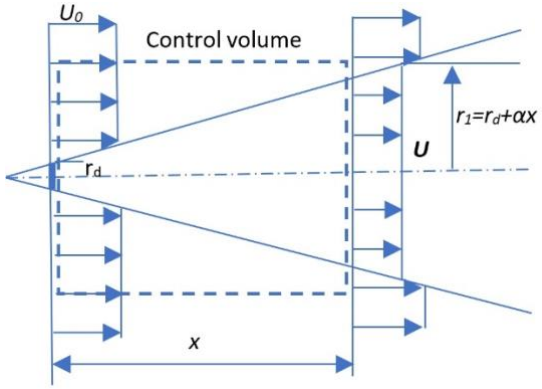

Fig. 4. Schematic diagram of the Jensen wake model.

Here, power output is calculated using Eq. (3)

$$p_i = \eta \frac{1}{2} \rho A u_i^3 \tag{3}$$

where p_i, η, ρ, A, and u are the power output of wind turbine in watt, Betz Constant, air density in kg/m^3, wind turbine rotor swept area in m^2, and wind speed in m/s, respectively. The Betz constant cannot exceed 0.59. In the Jensen model, wake radius, r_ω is calculated using Eq. (4)

$$r_\omega = r_d + \alpha x \tag{4}$$

where r_ω, r_d, α, x is wake radius, wake radius immediately behind the turbine, entrainment constant, and downstream distance, respectively. The calculation of the entrainment constant (α) reflects the speed of wake expansion given by Eq. (5)

$$\alpha = \frac{0.5}{\log\left(\frac{z}{z_0}\right)} \tag{5}$$

where z, and z_0 is hub height and surface roughness considered constant in the current work, respectively. To calculate wake radius r_d behind the turbine, Eq. (6) is used as follows:

$$r_d = r_0 \sqrt{\frac{1-\alpha}{1-2a}} \tag{6}$$

where r_0 is rotor radius, and a is axial induction factor.

The wind slows down as it approaches the turbine. The ratio of this reduced wind speed and free stream velocity, u_0, is axial induction factor, a, calculates use the Thrust Coefficient c_t, as given in Eq. (7)

$$c_t = 4a\left(1-a\right) \tag{7}$$

laying between latitudes 12°N and 120°S with an optimum temperature of between 24 – 38°C, average radiation of 5-7

$$\frac{u_\omega}{u_0} = \left(1 - \frac{2a}{\left(1+\frac{ax}{r_d}\right)^2}\right) \tag{8}$$

where u_ω is wake velocity and u_0 is free velocity.

Eq. (8) is used for a single wind turbine in the Jensen wake model. Builtjes et al. [33] researched the calculation of the wake effect on the wind turbine farm by defining the ratio of the average energy output of a wind turbine positioned in a farm and the energy output of an isolated wind turbine as the formula:

$$P(n) = \frac{P}{P_0} \tag{9}$$

where $P(n)$ is the ratio of the average energy output to the isolated single wind turbine of the n-th wind turbine due to the wake effect, P is the average power of the wind turbine in a wind farm and P_0 is the power of an isolated single wind turbine. In a simple way, we define the wake value based on the differentiation of down spacing from Eq. (9) become the following equation.

$$\omega(n) = 1 - P(n) \tag{10}$$

The Builtjes' experiments done on the WT farm by the down spacing of 2D, 5D, 7D, 10D, and 20D with the variation of degrees in 0°, 5°, 15°, and 30° as shown in Fig. 5.

We redefine Fig. 5 and Eq. (10) to Table 2.

Table 2. The ω value in the various down spacing and the upwind direction.

Down spacing	The direction to the upwind	*P(n)*	*ω = 1 - P(n)*
2D	0°	0.15	0.85
2D	5°	0.22	0.78
2D	15°	0.4	0.6
2D	30°	0.95	0.05
5D	0°	0.3	0.7
5D	10°	0.7	0.3
7D	0°	0.35	0.65
7D	10°	0.71	0.29
7D	15°	0.88	0.12
10D	0°	0.57	0.43
10D	5°	0.86	0.14
20D	0°	0.84	0.16

2.5. The Genetic Algorithm Optimization

The objective function is to minimize the total wake effect of the wind turbine farm as defined by Eq. (11)

$$\omega_{total} = \sum_{m=2}^{6} \sum_{n-1}^{10} \omega_{(m,n)} x_{(m,n)} x_{(m-1,n)} \tag{11}$$

where ω_{total} is wake effect of all installed wind turbines, $\omega_{(m,n)}$ is a wake constant for a wind turbine in the *m* rows and *n* columns, *m* is wind turbine in rows, *n* is wind turbine in columns, and $x_{(m-1,n)}$ is the existence of wind turbine in the previous row *m* and column *n*.

The wake constant refers to Table 2, with only using 2D and 5D downwind spacing on this study. The wake calculation starts from the second row of the Wind Turbine Generator (WTG) farm with the assumption that is wake effect on the first row is zero since there is no obstacle from the upwind direction.

We used two constraints on this optimization; the first is the limitation of the total capacity of the WTG and the second is the priority and nonpriority location value based on Fig. 3 (b) for the single wind turbine on the location $x_{(m,n)}$. The matrix size is (6,10) means 6 rows and 10 columns with the binary value 0 and 1 for the location $x_{(m,n)}$. The value of 0 means the non-existence of WTG and 1 means the existence of a single WT for the location $x_{(m,n)}$.

The wind farm has singular capacities, which means using the same capacities for a single wind turbine. In this study, we proposed 90 kW, 150 kW, 225 kW, and 250 kW for a single wind turbine. On results, we have four scenarios of a WTG's configuration based on its single WTG capacity.

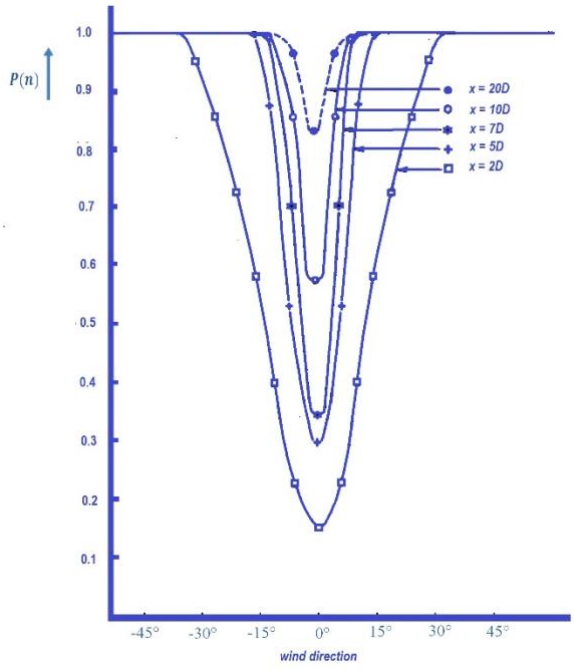

Fig. 5. The wake effect of wind turbine [33].

3. Results and Discussions

2.6. Variations of Wind Speed

Knowledge of wind variations at a site is required to demonstrate the seasonal behavior of wind speed at a specific location. Such differences are critical for the design and selection of suitable wind turbines, energy storage, and scenario planning. Figure 6 depicts these variations. Figure 6 (a) depicts how the wind fluctuates significantly throughout the day and night based on 12 months of data collected at 33 m. There are 10-minute intervals with wind speeds of less than 3 m/s, as seen. Similarly, wind speeds can exceed 10 m/s at times.

A box plot representing the monthly maximum wind speed, average daily high, average daily low, and monthly mean wind speed of the data gathered at altitudes of 34 m is displayed in Fig. 6 (b). Maximum wind power may be captured due to the faster speed. The figure clearly shows that from June to August, the wind speed is higher. The box plot can also be used to identify outliers for a typical thunderstorm wind.

Figure 6 (c) shows the average monthly wind speed for Hambapraing. From the graph, it is clear that there are significant monthly variations in average wind speed. While June through August have the strongest seasonal prevailing winds, October through December have the lowest wind speeds. Due to the fact that it offers a reliable estimate of the amount of electricity a wind farm can supply to the power system in a given month, this information is essential for wind farm installation. This research was carried out in Hambapraing, East Sumba Regency. Sumba Island has a semi-arid climate type with a short rainy season that lasts only for four months (December to March) and a total annual rainfall of 547 mm.

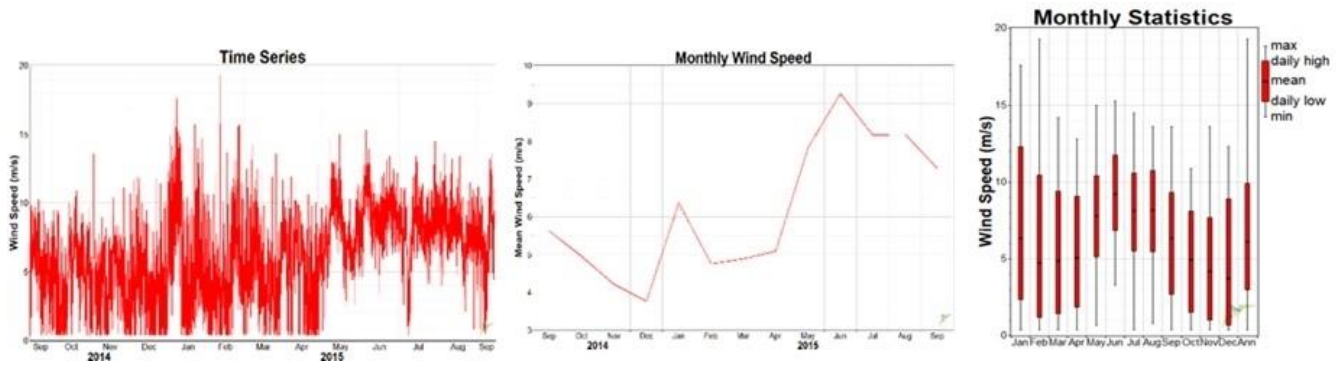

(a) (b) (c)

Fig. 6. Variation of wind speed: (a) time series, (b) monthly mean wind speed, and (c) monthly boxplot statistic.

2.7. Wind Direction

The dominant wind direction is crucial when assessing a wind energy resource and looking for ideal locations to put wind turbines [34]. If most of the wind energy moves in one direction, there shouldn't be any obstructions or interference in the path of the wind. The wind generator's orientation needs to be perpendicular to the wind's direction to capture the most wind energy possible [27]. Figure 7 depicts the annual and monthly sector-wise distribution of wind roses, divided into 16 distinct portions spaced at 22,50 consecutive intervals. It was found that the dominant strong winds for the entire year come from the southeast sector. The dominant wind direction is northwest from December to March and southeast for the remaining eight months.

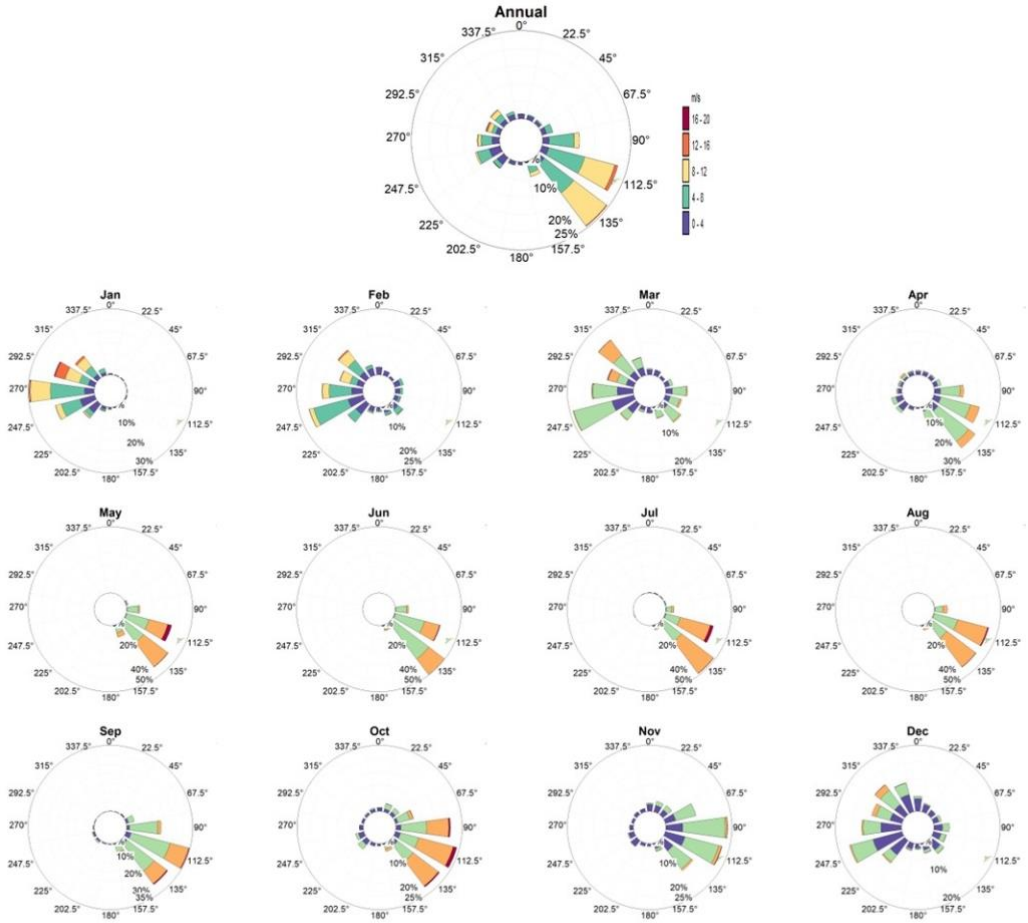

Fig. 7. Annual and monthly wind rose profile

2.8. Wind Diurnal

A certain location's wind speed varies throughout the day. The behavior of wind speed over the course of a year is examined using the diurnal profile. The wind speed does not significantly vary throughout the year; however, it is a little bit higher during the day than at night (see Fig. 8). The average wind speed is lowest at 6 a.m., then increases and peaks around 12 p.m. from January to April and September to December. In May–August, the average wind speed exceeds 7 m/s throughout the day.

2.9. Weibull Frequency Distribution and Wind Power Density (WPD)

Table 3 shows the annual and monthly Weibull's shape parameters k and scale c, as well as the WPD. The scale parameter can be used to indicate wind strength, whereas the shape parameter can be used to indicate wind stability and distribution at a specific location. WPD is one of the best indicators of wind resources because it considers the frequency distribution of wind velocity, air density, and the cube of wind speed. According to the table, the lowest shape parameter during the study was 1.59 in February and the highest was 5.15 in June. The lowest value of the scale parameter, on the other hand, was 4.31 in December, and the highest was 9.61 in June. The highest WPD was recorded in June, at 484.8 W/m^2, while the lowest was recorded in December, at 72.0 W/m^2. Therefore, the wind potentiality is lowest in December, increases until it reaches its peak in June, and then begins to fall again. The overall 1-year measurement at Hambapraing yielded the Weibull's shape parameter k = 2.67, the scale parameter c = 7.04 m/s, and the WPD = 225.4 W/m^2. Figure 9 depicts the Weibull distribution frequencies for the entire year and monthly at an altitude of 34 m. The power produced by the on-site wind turbine can be predicted using these frequencies. Throughout the year, the most frequent speeds were between 5 and 10 m/s. Strong winds occur from June to August, with the most frequent speeds appearing to be between 8 and 9 m/s.

Table 3. Weibull's parameters and WPD.

Down spacing	Weibull Parameter		WPD (W/m^2)
	k	c (m/s)	
Annual	2.67	7.04	225.4
January	1.92	7.05	299.0
February	1.59	5.05	142.4
March	1.96	5.33	125.9
April	2.85	6.01	135.9
May	3.43	8.31	335.4
June	5.15	9.61	484.8
July	5.09	8.69	358.2
Augustus	4.80	8.55	342.8
September	3.22	6.98	203.1
October	3.03	5.78	118.0
November	2.53	4.92	79.8
December	1.84	4.31	72.0

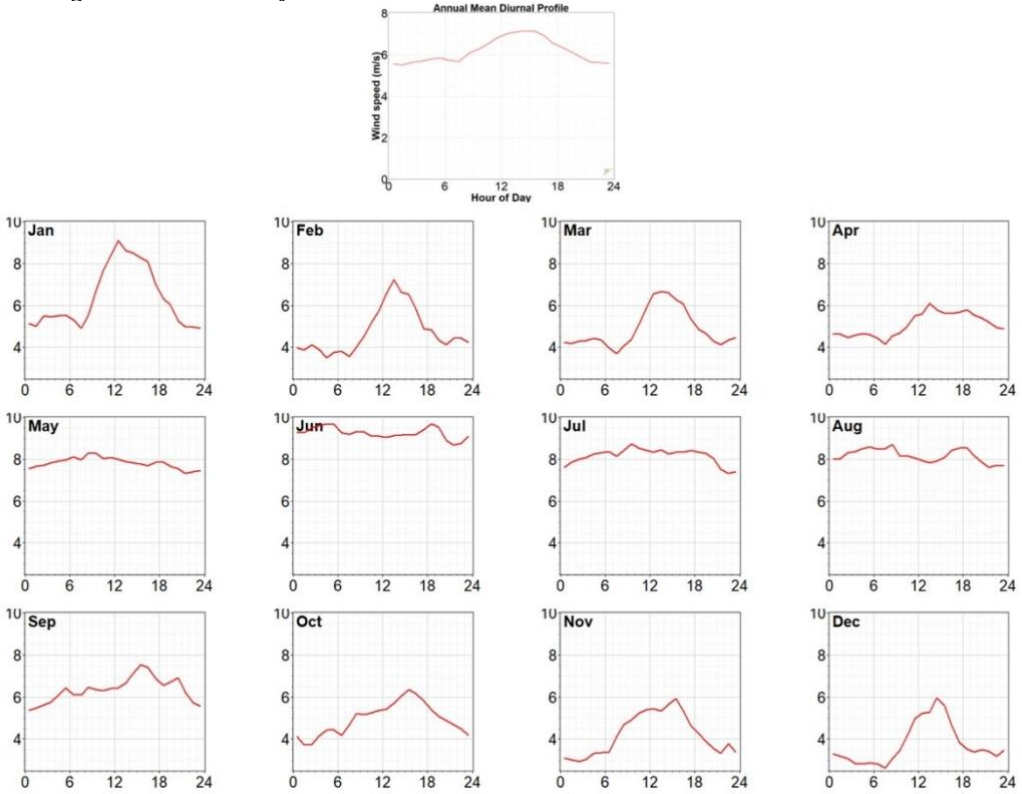

Fig. 8. Annual and monthly mean diurnal profiles in Hambapraing.

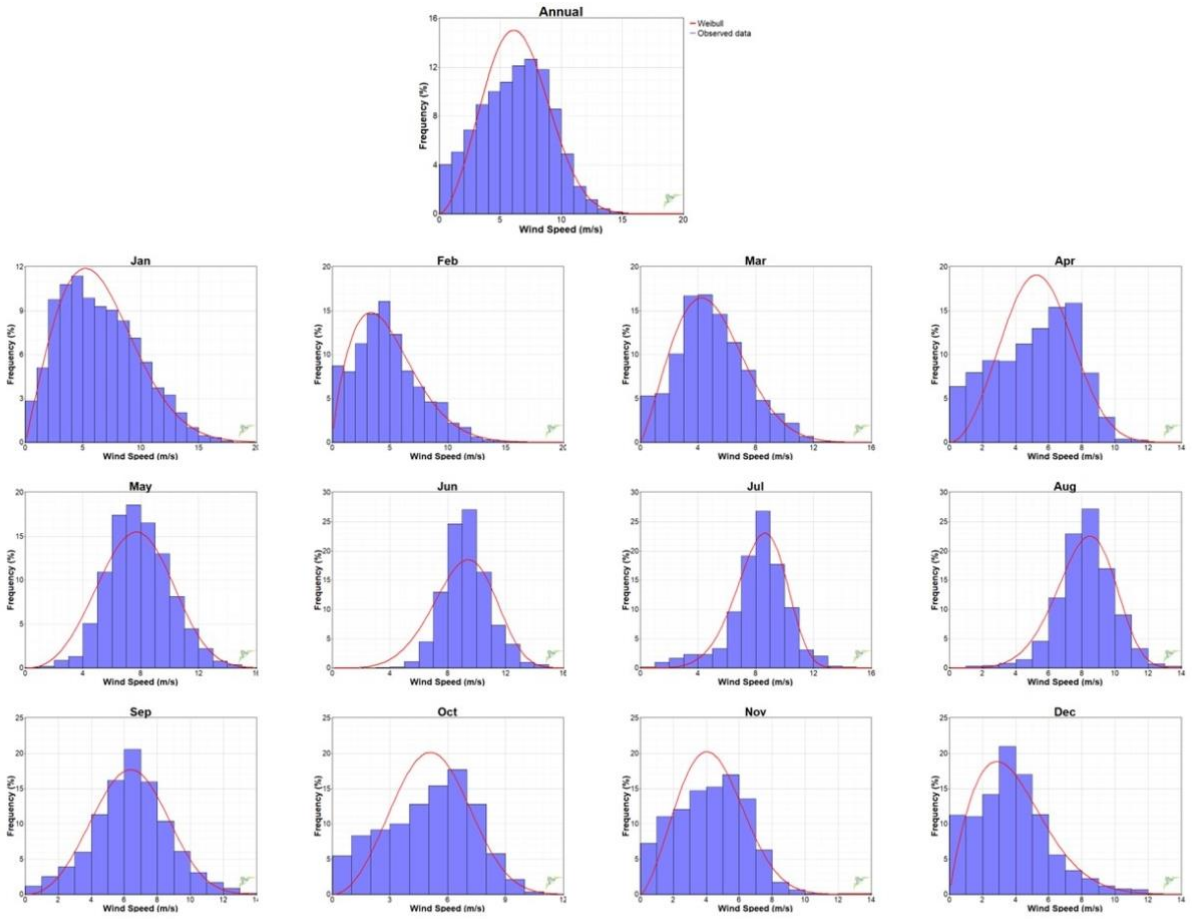

Fig. 9. Annual and monthly Weibull frequency distribution.

2.10. Optimization Results in WTGs' Array

Figure 10 shows the optimal result of micro-siting WTG with identical 90 kW, 150 kW, 225 kW, and 250 kW as Scenario 1, 2, 3, and 4, respectively. Using the software Arc GIS 10.8 and WAsP version 12.7, Fig. 11, Fig. 12. Fig. 13, and Fig. 14 show a location map and the layouts of Scenario 1, Scenario 2, Scenario 3, and Scenario 4, respectively, for the wind turbine. It is based on optimization calculations in the East Sumba Regency of East Nusa Tenggara Province using the Universal Transverse Mercator (UTM) system coordinates for Zone 51. Scenario 1 is a configuration of 34 wind turbines with a capacity of 90 kW each; Scenario 2 is a configuration of 20 wind turbines with a capacity of 150 kW each; Scenario 3 is a configuration of 14 wind turbines with a capacity of 225 kW each; and Scenario 4 is a configuration of 12 wind turbines with a capacity of 250 kW each.

By using WAsP version 12.7, the results of the calculations for the four scenarios can be seen in Table 4-8. From Table 4-8, it can be seen that Scenario 1, with a configuration of 34 WTGs, produces the largest total net AEP of 11,287 MWh/yr with a wake loss of 3.73%. The wake loss and total net AEP for Scenarios 2 and 3 are 3.6%, 10,742 MWh/yr, and 2.98%, 11,429 MWh/yr, respectively. Scenario 4 has the lowest wake loss of 2.62% and produces a net AEP of 10,221 MWh/yr.

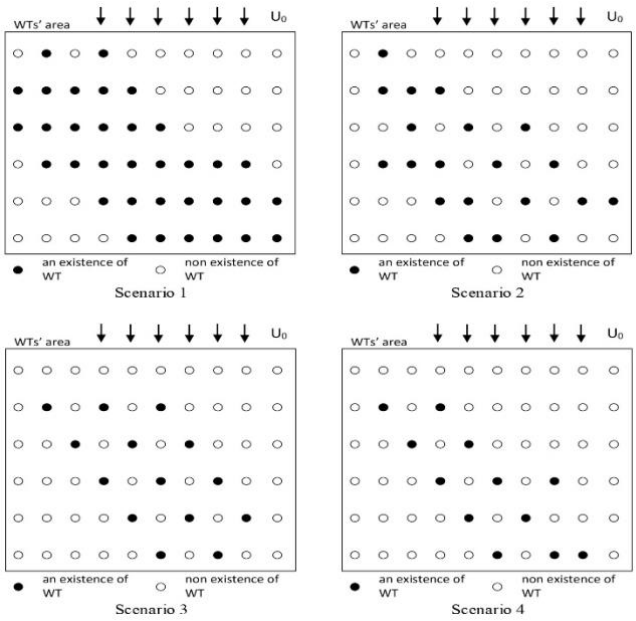

Fig. 10. Configuration of identical WTG in various scenarios.

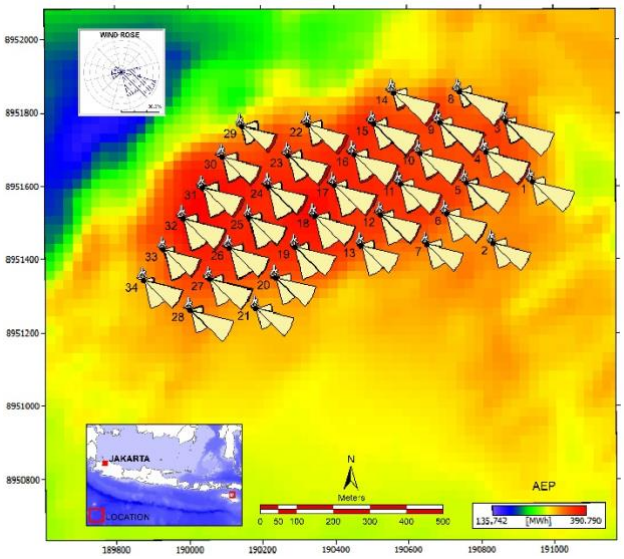

Fig. 11. Scenario 1.

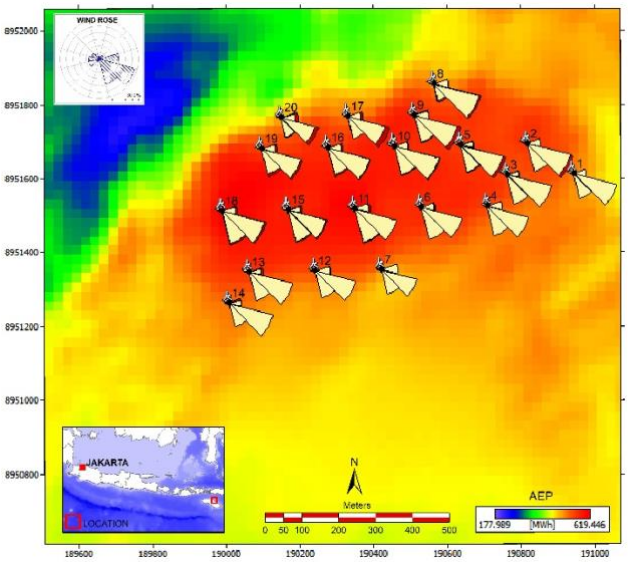

Fig. 12. Scenario 2.

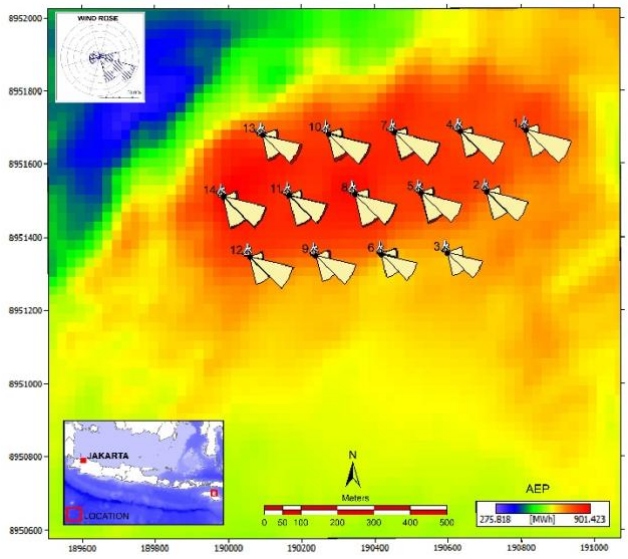

Fig. 13. Scenario 3.

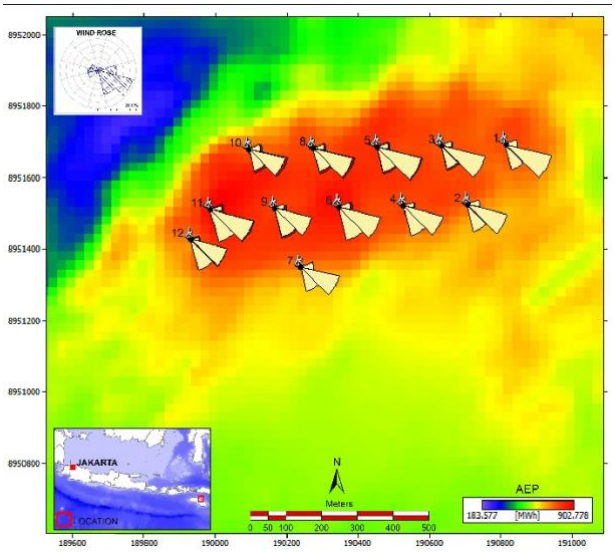

Fig. 14. Scenario 4.

Table 4. Turbine coordinates, wake loss, Gross and Net AEP for Scenario 1.

Number of turbine	X-UTM51S	Y-UTM51S	Wake loss (%)	Gross AEP (MWh/yr)	Net AEP (MWh/yr)
1	190940	8951613	1.3	323	318
2	190832	8951444	1.27	322	318
3	190867	8951778	1.59	341	336
4	190813	8951694	2.32	351	343
5	190760	8951610	2.4	344	335
6	190706	8951525	2.51	345	337
7	190652	8951441	1.78	331	325
8	190741	8951859	3.09	318	308
9	190687	8951774	3.85	350	336
10	190633	8951690	4.1	347	333
11	190579	8951606	3.93	360	346
12	190526	8951522	3.17	356	345
13	190472	8951438	1.88	345	339
14	190561	8951855	5.02	318	302
15	190507	8951771	4.57	361	345
16	190453	8951687	4.57	366	350
17	190399	8951603	4.21	370	355
18	190345	8951518	3	382	371
19	190292	8951434	1.8	368	361
20	190238	8951350	1.28	341	336
21	190184	8951266	1.01	311	307
22	190327	8951768	6.21	323	303
23	190273	8951684	5.22	353	335
24	190219	8951599	4.44	366	350
25	190165	8951515	3.85	362	348
26	190111	8951431	3.33	365	353
27	190057	8951347	2.54	352	343
28	190004	8951262	1.07	324	321
29	190146	8951764	6.71	303	283
30	190093	8951680	5.41	345	327
31	190039	8951596	4.31	379	363
32	189985	8951512	3.7	384	370
33	189931	8951427	3.93	336	323
34	189877	8951343	2.74	316	308

Table 5. Turbine coordinates, wake loss, Gross and Net AEP for Scenario 2.

Number of turbine	X-UTM51S	Y-UTM51S	Wake loss (%)	Gross AEP (MWh/yr)	Net AEP (MWh/yr)
1	190943	8951613	1.52	519	511
2	190817	8951694	2.95	562	546
3	190763	8951609	2.41	553	540
4	190709	8951525	1.34	557	550
5	190636	8951690	6.09	559	525
6	190529	8951522	2.03	575	564
7	190421	8951353	1.15	520	514
8	190564	8951855	4.46	512	489
9	190510	8951771	5.38	579	548
10	190456	8951687	4.54	589	562
11	190349	8951518	3.19	614	595
12	190241	8951350	1.81	552	542
13	190061	8951347	1.65	568	558
14	190007	8951262	0.34	525	523
15	190168	8951515	4.47	585	559
16	190276	8951683	4.91	570	542
17	190330	8951768	6.88	524	488
18	189988	8951512	3.41	618	597
19	190096	8951680	5.4	559	529
20	190149	8951764	8.29	492	451

Table 6. Turbine coordinates, wake loss, Gross and Net AEP for Scenario 3.

Number of turbine	X-UTM51S	Y-UTM51S	Wake loss (%)	Gross AEP (MWh/yr)	Net AEP (MWh/yr)
1	190813	8951694	0.71	836	830
2	190706	8951525	1.15	825	816
3	190598	8951357	1.19	759	750
4	190633	8951690	2.89	832	808
5	190526	8951522	3.15	853	826
6	190418	8951354	2.11	779	763
7	190453	8951687	4.06	874	838
8	190345	8951518	3.63	912	878
9	190238	8951350	2.06	819	802
10	190273	8951683	5.15	847	803
11	190165	8951515	4.22	868	832
12	190058	8951347	1.62	842	828
13	190093	8951680	5.59	827	781
14	189985	8951512	3.74	909	875

4. Conclusion

In this work, an optimization method for minimizing the total wake effect of a wind turbine farm on the island of Sumba, Indonesia, using a genetic algorithm is developed and simulated with WaSP software to estimate the AEP. The wind farm layout and preliminary turbine micrositing were completed with various scenarios in mind to achieve the best possible result. Four different scenarios are considered to maximize power output. There are 34 identical wind turbine generators (WTG) with a unit capacity of 90 kW in Scenario 1. Scenario 2 includes 20 identical wind turbine generators with a total capacity of 3000 kW. In Scenario 3, 14 identical WTG with 225 kW of unit capacity are used. In Scenario 4, there are 12 identical WTGs with a unit capacity of 250 kW. The results showed that Scenario 1 produced the highest total net AEP of 11,287 MWh/year with a 3.73% wake loss. The minimum wake loss seemed to be 2.62% in Scenario 4, with a total net AEP of 10,221 MWh/year.

Table 7. Turbine coordinates, wake loss, Gross and Net AEP for Scenario 4.

Number of turbine	X-UTM51S	Y-UTM51S	Wake loss (%)	Gross AEP (MWh/yr)	Net AEP (MWh/yr)
1	190813	8951694	0.58	854	849
2	190706	8951525	0.97	843	835
3	190633	8951690	3.19	856	828
4	190526	8951522	1.85	877	861
5	190453	8951687	4.16	903	865
6	190345	8951518	1.84	946	928
7	190238	8951350	0.64	838	832
8	190273	8951683	5.12	869	825
9	190165	8951515	3.57	899	867
10	190093	8951680	5.79	844	795
11	189985	8951512	2.39	940	918
12	189931	8951427	1.25	828	818

Table 8. The proportional wake loss and Annual Energy Production for various scenarios.

Scenario	Number of Wind Turbine	Turbine Rating (kW)	Total Rating Capacity (kW)	Proportional wake loss (%)	Total gross AEP (MWh/yr)	Total net AEP (MWh/yr)
1	34	90	3060	3.73	11,681	11,287
2	20	150	3000	3.60	11,133	10,732
3	14	225	3150	2.98	11,780	11,429
4	12	250	3000	2.62	10,496	10,221

The findings of this study are one of the solutions to the proposed wind farm project in the same location by Win Rock International and NREL in 2015, which was delayed owing to the state of infrastructure and land transportation on the island. Because of these issues, we limited the wind turbine capacity to less than 500 kW.

This single-objective optimization has drawbacks in that it does not simultaneously investigate minimizing the total wake effect of the wind turbine farm and minimizing energy production costs. The investment cost includes not only the infrastructure of the WT towers and the cost of the land occupied but also the cost of connecting and maintaining grid stability between the WT generators and the load distributions. For future studies, we will investigate multi-objective optimization with a focus on the maximization of annual energy production and the simultaneous minimization of investment costs.

References

[1] M. A. Saeed, Z. Ahmed, S. Hussain, and W. Zhang, "Wind resource assessment and economic analysis for wind energy development in Pakistan," Sustain. Energy Technol. Assessments, vol. 44, p. 101068, April 2021.

[2] X. Y. Tang, S. Zhao, B. Fan, J. Peinke, and B. Stoevesandt, "Micro-scale wind resource assessment in complex terrain based on CFD coupled measurement from multiple masts," Appl. Energy, vol. 238, pp. 806–815, March 2019.

[3] C. Jung and D. Schindler, "Introducing a new approach for wind energy potential assessment under climate change at the wind turbine scale," Energy Convers. Manag., vol. 225, p. 113425, December 2020.

[4] N. W. Hesty, D. G. Cendrawati, R. Nepal, and M. I. Al Irsyad, "Wind Energy Potential Assessment Based-on WRF Four-Dimensional Data Assimilation System and Cross-Calibrated Multi-Platform Dataset," IOP Conf. Ser. Earth Environ. Sci., vol. 897, no. 1, pp. 0–7, November 2021.

[5] B. Pranoto, H. Soekarno, D.G. Cendrawati, I.F. Akrom, M.I.A. Irsyad, N.W. Hesty, Aminuddin, I. Adilla, L. Putriyana, A.F. Ladiba, Widhiatmaka, R. Darmawan, S.R. Fithri, R. Isdiyanto, V.J. Wargadalam, M. Magdalena, and M. Aman, "Indonesian hydro energy potential map with run-off river system," IOP Conf. Ser. Earth Environ. Sci., vol. 926, no. 1, November 2021.

[6] V. Nurliyanti, K. Ahadi, R. Muttaqin, B. Pranoto, G. P. Srikandi, and M. I. Al Irsyad, "Fostering Rooftop Solar PV Investments Toward Smart Cities through e-SMART PV," 5th Int. Conf. Smart Grid Smart Cities, pp. 146–150, June 2021.

[7] Winrock International, "Fuel Indenpendent Renewable Energy 'Iconic Island' Preliminary Resource Assessment Sumba & Buru Islands - Indonesia," 2010. [Online]. Available: https://www.bibalex.org/Search4Dev/document/437343 (accessed Mar. 9, 2023)

[8] I. Pramuwardani, Hartono, Sunarto, and A. Sopaheluwakan, "Indonesian rainfall variability during Western North Pacific and Australian monsoon phase related to convectively coupled equatorial waves," Arab. J. Geosci., vol. 11, no. 21, November 2018.

[9] I. Alifdini, T. Shimada, and A. Wirasatriya, "Seasonal distribution and variability of surface winds in the Indonesian seas using scatterometer and reanalysis data," Int. J. Climatol., vol. 41, no. 10, pp. 4825–4843, April 2021.

[10] R. Fisher, W. E. Bobanuba, A. Rawambaku, G. J. E. Hill, and J. Russell-Smith, "Remote sensing of fire regimes in semi-arid Nusa Tenggara Timur, eastern Indonesia: Current patterns, future prospects," Int. J. Wildl. Fire, vol. 15, no. 3, pp. 307–317, January 2006.

[11] B. Yulianto, S. Maarif, C. Wijaya, and H. Hardjomidjojo, "Energy Security Scenario based on Renewable Resources: A Case Study of East Sumba, East Nusa Tenggara, Indonesia," Bisnis Birokrasi J., vol. 26, no. 1, May 2019.

[12] M.C. Brower, B.H. Bailey, P. Beaucage, D.W. Bernadett, J. Doane, M.J. Eberhard, K. V. Elsholz, M. V. Filippelli, E. Hale, M.J. Markus, D. Ryan, M.A. Taylor, and J.C. Tensen, "Wind Resource Assessment: A Practical Guide to Developing a Wind Project," John Wiley & Sons, Ltd, May 2012.

[13] E. P. P. Soares-Ramos, L. De Oliveira-Assis, R. Sarrias-Mena, P. Garcia-Trivino, C. A. Garcia-Vazquez, and L. M. Fernandez-Ramirez, "Control of a Grid-connected Wind Turbine with Quasi-Z-Source Inverter," in 9th International Conference on Renewable Energy Research and Applications, pp. 309–314, September 2020.

[14] S. Mathew, Wind energy: Fundamentals, resource analysis and economics. New York: Springer-Verlag, March 2006.

[15] J. F. Manwell, J. G. McGowan, and A. L. Rogers, Wind Energy Explained: Theory, Design and Application, Second Edition, John Wiley & Sons, Ltd, December. 2009.

[16] M. Djamai and N. Kasbadji Merzouk, "Wind farm feasibility study and site selection in Adrar, Algeria," Energy Procedia, vol. 6, pp. 136–142, April 2011.

[17] R.G.J. Flay, A.B. King, M. Revell, P. Carpenter, R. Turner, P. Cenek, and A.A. Safaei Pirooz, "Wind speed measurements and predictions over Belmont Hill, Wellington, New Zealand," J. Wind Eng. Ind. Aerodyn., vol. 195, p. 104018, December 2019.

[18] U. Yilmaz, F. Balo, and L. S. Sua, "Simulation Framework for Wind Energy Attributes with WAsP," Procedia Comput. Sci., vol. 158, pp. 458–465, June 2019.

[19] I. Kamdar, S. Ali, J. Taweekun, and H. M. Ali, "Wind farm site selection using WAsP tool for application in the tropical region," Sustain., vol. 13, no. 24, December 2021.

[20] P. Ratjiranukool and S. Ratjiranukool, "Evaluating Wind Speed by WRF Model over Northern Thailand," Energy Procedia, vol. 138, pp. 1171–1176, October 2017.

[21] Z. Wang and W. Liu, "Wind energy potential assessment based on wind speed, its direction and power data," Sci. Rep., vol. 11, no. 1, pp. 1–15, August 2021.

[22] S. D. Kwon, "Uncertainty analysis of wind energy potential assessment," Appl. Energy, vol. 87, no. 3, pp. 856–865, March 2010.

[23] A. Geçmez and Ç. Gençer, "Wind Energy Production Estimation with ANN and ANFIS," 9th International Conference on Smart Grid, October 2021.

[24] O. Ozturk, B. Hangun, and M. Shoaeinaeini, "Utilizing Machine Learning to Predict Offshore Wind Farm Power Output for European Countries," 11th International

Conference on Renewable Energy Research and Application, October 2022.

[25] F. H. Mahmood, A. K. Resen, and A. B. Khamees, "Wind characteristic analysis based on Weibull distribution of Al-Salman site, Iraq," Energy Reports, vol. 6, pp. 79–87, February 2020.

[26] F. Azlan, J. C. Kurnia, B. T. Tan, and M. Z. Ismadi, "Review on optimisation methods of wind farm array under three classical wind condition problems," Renew. Sustain. Energy Rev., vol. 135, p. 110047, January 2021.

[27] H. S. Ramadan, "Wind energy farm sizing and resource assessment for optimal energy yield in Sinai Peninsula, Egypt," J. Clean. Prod., vol. 161, pp. 1283–1293, September 2017.

[28] D. Romanic, D. Parvu, M. Refan, and H. Hangan, "Wind and tornado climatologies and wind resource modelling for a modern development situated in 'Tornado Alley,'" Renew. Energy, vol. 115, pp. 97–112, January 2018.

[29] A. Hossieni, V. Rasouli, and S. Rasouli, "Wind energy potential assessment in order to produce electrical energy for case study in Divandareh, Iran," in 3rd International Conference on Renewable Energy Research and Applications, pp. 133–137, October 2014.

[30] P. Tiam Kapen, M. Jeutho Gouajio, and D. Yemélé, "Analysis and efficient comparison of ten numerical methods in estimating Weibull parameters for wind energy potential: Application to the city of Bafoussam, Cameroon," Renew. Energy, vol. 159, pp. 1188–1198, October 2020.

[31] E. Rodrigo and A. Larico, "Wind Energy Potential by the Weibull Distribution at High-Altitude Peruvian Highlands," Int. J. Smart grid, vol. 5, no. 3, September 2021.

[32] M. Bin Ali, Z. Ahmad, S. Alshahrani, M. R. Younis, I. Talib, and M. Imran, "A Case Study: Layout Optimization of Three Gorges Wind Farm Pakistan, Using Genetic Algorithm," Sustain., vol. 14, no. 24, December 2022.

[33] P. J. H. Builtjes and J. Smit., "Calculation of Wake Effects in Wind Turbine Parks," in Wind Engineering, vol. 2, no. 3, Sage Publications, Ltd., 1978, pp. 135–145.

[34] V. Sharma, M. Calaf, M. Lehning, and M. B. Parlange, "Time-adaptive wind turbine model for an LES framework," Wind Energy, vol. 19, no. 5, pp. 939–952, May 2016.